Lipid Envelope-Type Nanoparticle Incorporating a Multifunctional Peptide for Systemic siRNA Delivery to the Pulmonary Endothelium

Kenji Kusumoto,[†] Hidetaka Akita,[‡] Taichi Ishitsuka,[‡] Yu Matsumoto,[§] Takahiro Nomoto,[⊥] Ryo Furukawa,[‡] Ayman El-Sayed,[‡] Hiroto Hatakeyama,[‡] Kazuaki Kajimoto,[‡] Yuma Yamada,[‡] Kazunori Kataoka,[§,⊥,*] and Hideyoshi Harashima[‡,*]

[†]Laboratory for Formulation Research, Taiho Pharmaceutical Co., Ltd., 224-2 Ebisuno, Hiraishi, Kawauchi-cho, Tokushima 771-0194, Japan, [‡]Laboratory for Molecular Design of Pharmaceutics, Faculty of Pharmaceutical Sciences, Hokkaido University, Kita-12, Nishi-6, Kita-ku, Sapporo 060-0812, Japan, [§]Division of Clinical Biotechnology, Center for Disease Biology and Integrative Medicine, Graduate School of Medicine, The University of Tokyo, 7-3-1 Hongo, Bunkyo-ku, Tokyo, 113-8656, Japan, and [⊥]Department of Bioengineering, Graduate School of Engineering, The University of Tokyo, 7-3-1 Hongo, Bunkyo-ku, Tokyo, 113-8656, Japan. Kenji Kusumoto and Hidetaka Akita equally contributed to this study.

ABSTRACT

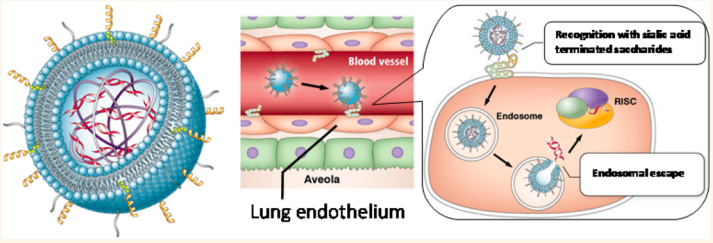

A system that permits the delivery of cargoes to the lung endothelium would be extraordinarily useful in terms of curing a wide variety of lung-related diseases. This study describes the development of a multifunctional envelope-type nanodevice (MEND) that targets the lung endothelium, delivers its encapsulated siRNA to the cytoplasm, and eradicates lung metastasis. The key to the success can be attributed to the presence of a surface-modified GALA peptide that has dual functions: targeting the sialic acid-terminated sugar chains on the pulmonary endothelium and subsequently delivering the encapsulated cargoes to the cytosol *via* endosomal membrane fusion, analogous to the influenza virus. The active targeting of MENDs without the formation of large aggregates was verified by intravital real-time confocal laser scanning microscopy in living lung tissue. The GALA-modified MEND is a promising carrier that opens a new generation of therapeutic approaches for satisfying unmet medical needs in curing lung diseases.

KEYWORDS: lung endothelium targeting · siRNA · GALA · real-time imaging · nanoparticles

Current studies have shown that physiological perturbation of the pulmonary endothelium is closely related to a variety of severe and life-threatening lung disease (cancer,[1] sepsis,[2] acute lung injury/acute respiratory distress syndrome,[3] and pulmonary hypertension[3,4]). Therefore, the targeted delivery of nucleic acids (small interfering RNAs (siRNAs) and microRNAs (miRNAs)) to the lung endothelium is a highly promising strategy for addressing currently unmet medical needs.[1,2,5] Traditional nonviral vectors to lung targeting involve the use of cationic materials (lipoplex or polyplex) since cationic charge is a crucial driving force for the cellular binding and subsequent endosomal escape.[6−8] However, this strategy is attended by risks, since temporal trapping in microvessels, concomitant with the formation of large aggregates with erythrocytes, is a major driving force for lung accumulation.[9,10] The large aggregates with erythrocytes may cause clinical problems because of microinfarctions, causing tissue ischemia and possible myocardial damage.[11] In this study, we report on the development of an artificial carrier for the cytoplasmic delivery of encapsulating RNA (siRNA) into

* Address correspondence to (K. Kataoka) kataoka@bmw.t.u-tokyo.ac.jp; (H. Harashima) harasima@pharm.hokudai.ac.jp.

Received for review March 15, 2013 and accepted August 3, 2013.

Published online August 03, 2013
10.1021/nn401317t

the lung endothelium *via* active targeting without any aggregation in the bloodstream.

For successful siRNA delivery, targeting of the specific cells and subsequent cytoplasmic delivery (endosomal escape) is one of the crucial rate-limiting processes for the delivery of siRNA. Along with the long evolution of life, viruses have also evolved and have developed elegant mechanisms for the cytoplasmic transport of their genomic DNA or RNA. One such example is the influenza virus, an envelope-type RNA virus that delivers its RNA genome after fusion of the envelope to the endosomal/lysosomal membrane. In this process, hemagglutinin 2 (HA2), which is present on the viral lipid envelope, plays a key role in membrane fusion by changing its conformation in response to the acidic environment.[12,13] The design of our particle, which we refer to as a multifunctional envelope-type nanodevice (MEND), was inspired by the influenza virus; the critical structural elements include a nucleic acid/polycation condensed core coated with liposomal envelopes.[14,15] The most significant success in this study was the novel discovery of the function of its on-board peptide, GALA (WEAALAEALAEALAEHLAEALAEALEALAA),[16] a peptide originally developed as an endosomal destabilizer, inspired by the mechanism of HA2 in the influenza virus. The structure of this peptide also adopts an α-helical conformation when exposed to the acidic pH in endosomes. Conjugation of cholesterol to the GALA (Chol-GALA) allows anchoring to the lipid bilayer so that the GALA becomes spontaneously oriented outward from the surface of the lipid envelope[17] (Figure 1A). To apply this peptide for *in vivo* use, we attempted to modify a certain kind of ligand peptide (*i.e.*, IRQ peptide) along with Chol-GALA.[18] However, in the process of the optimization of these systems, we serendipitously found that GALA peptide itself has an additional function as a ligand for the lung endothelium. The objective of the present study was to clarify the mechanism and/or driving force for the accumulation of GALA-modified MEND (GALA-MEND) in the lung, which can be distinguished from those of the conventional cationic lipoplex. To achieve this goal, we directly visualized the dynamic flow of GALA-MEND in the lung vasculature by means of intravital real-time confocal laser scanning microscopy (IVRTCLSM) in living mice.[19] Furthermore, the targeting

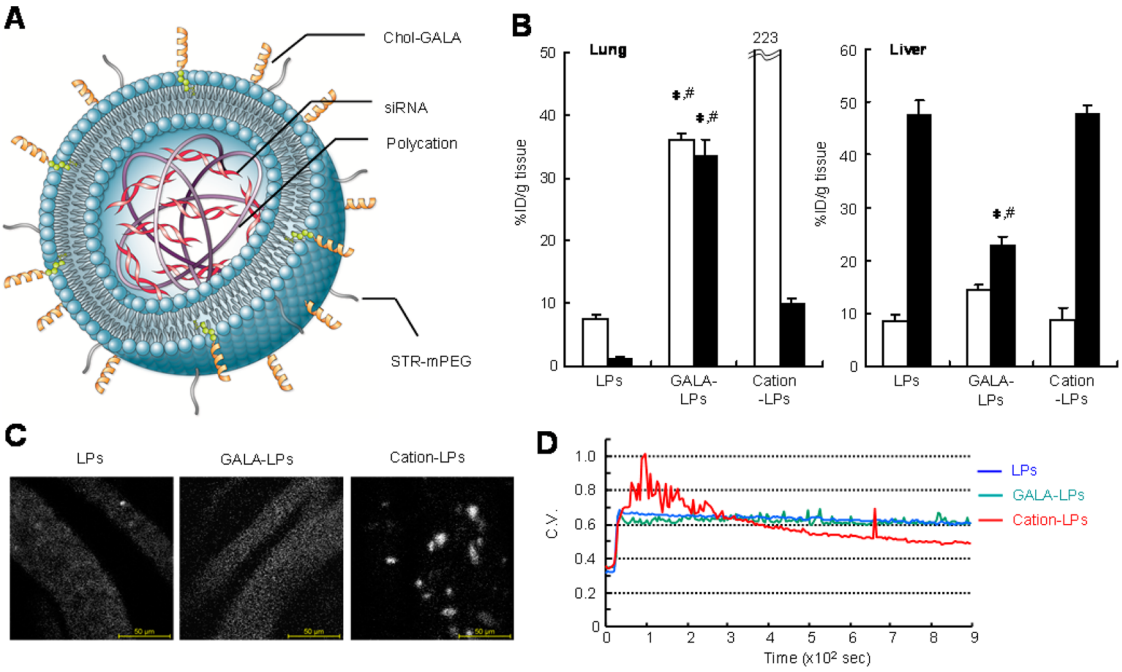

Figure 1. ***In vivo*** **disposition of GALA-modified liposomes. (A) Schematic illustration of the artificial influenza virus-like vector, GALA/MEND, for RNAi therapy. The elemental structure is a complex of siRNA and polyethyleneimine (PEI), encapsulated in a cationic liposomal envelope (DOTMA/EPC/Chol), the surface of which was modified with cholesteryl GALA (Chol-GALA) and STR-mPEG2000. (B) Biodistribution of the liposomes in lung (left) and liver (right). [^{3}H]CHE-labeled neutral liposomes (EPC/Chol) with or without modification by Chol-GALA (LPs and GALA-LPs, respectively) and cationic liposomes (cation-LPs) were iv administered to the mice. The distributions of liposomes after 5 and 360 min (open bars and solid bars) are represented as a percentage of the injected dose administered per g of tissue (%ID/g tissue, mean ± SE, n = 4). Statistical differences were evaluated by one-way ANOVA followed by Dunnett's test (*p < 0.01 *vs* LPs and $^{\#}p$ < 0.01 *vs* cation-LPs each time). (C) Intravital confocal microvideography of liposomes in the bloodstream of the mouse earlobe. Image frames (2.2 min after liposomes labeled with rhodamine were iv administered) were extracted from Supplemental Movies 1−3. (D) Aggregates were quantified based on the coefficient of variation (CV) of rhodamine fluorescence intensities in the frames extracted at 5 s intervals from crude Supplemental Movies 1−3. The degree of aggregation was quantified by calculating the CV of rhodamine fluorescence, which denotes the ratio of the standard deviation to the mean in the ROI cropped within a vessel region. The calculated CV values were plotted against time.**

molecules of GALA were identified. The second goal was to demonstrate the therapeutic activity of siRNA-encapsulated GALA-MEND to eradicate lung metastasis.

RESULTS AND DISCUSSION

Lung Accumulation. As a simplified demonstration, we investigated the impact of GALA modification on the pharmacokinetics of liposomes. Since neutral liposomes do not substantially accumulate in the lung (Figure 1B) or are poorly taken up by cells nonspecifically, we used a neutralized liposome composed of egg phosphatidylcholine (EPC)/cholesterol (chol)/stearyl-polyethylene glycol 2000 (STR-mPEG) as a basement particle to clearly demonstrate the functions as a targeting ligand to the lung endothelium. Modification of nanosized conventional liposomes (approximately 100 nm) with Chol-GALA reduced the ζ-potentials from -7 mV to -23 mV, since GALA is a negatively charged peptide that contains seven glutamic acid residues. Figure 1B shows data for the accumulation of tritium-labeled GALA-modified and unmodified liposomes ([^{3}H]GALA-LPs and [^{3}H]LPs, respectively) in the lung and liver at 5 and 360 min after iv administration. More detailed time profiles for the tissue distribution are shown in Figure S1. Of note, the association of GALA-LPs with lung tissue was approximately 24-fold higher than that of ordinary LPs at 360 min after their administration; GALA-LPs accumulated rapidly in the lung (within 5 min), and the levels remained constant thereafter for 360 min, while the levels of LPs decreased to nearly background values. Effective lung targeting by GALA-LPs was also supported by the finding that accumulation in the liver, which is commonly considered to be the major organ for clearing liposomes, was much lower. In traditional approaches using cationic materials, temporal trapping in microvessels, concomitant with the formation of large aggregates, is a major driving force for lung accumulation.[9,10,20] Thus, the biodistribution of tritium-labeled cationic liposomes composed of *N*-[1-(2,3-dioleyloxy)propyl]-*N*,*N*,*N*-trimethylammunium chloride (DOTMA)/EPC/Chol/STR-mPEG ([^{3}H]cation-LPs) was examined as an additional control. The pattern of the lung accumulation and retention was clearly different from that for [^{3}H]GALA-LPs; cation-LPs accumulated rapidly in the lung at 5 min, but their levels decreased substantially as early as 1 h postinjection, while the levels in the liver increased. These data suggest that the GALA-LPs accumulate in the lung by a mechanism different from that for cationic liposomes, which are mediated by the temporal entrapment of aggregatges in lung capillaries.

IVCLSM Imaging for the Dynamic Flow of Liposomes in Earlobe Blood Vessel. To gain more insights into the dynamics of the liposomes in the bloodstream, rhodamine-labeled liposomes were directly visualized by IVRTCLSM in earlobe blood vessels[19] (Supplemental Movies 1−3). Some examples of extracted frames (2.2 min after iv administration) are shown in Figure 1C. The cation-LPs became agglomerated into clumps in the micrometer range. In contrast, in the case of the LPs and GALA-LPs, the signals were dispersed. The degree of aggregation was quantified by calculating the coefficient of variation (CV) of the rhodamine fluorescence[21] (Figure 1D). The CV values of the cation-LPs subsequently fluctuated and decreased over time. In contrast, the CV values for the LPs and GALA-LPs remained at a plateau at lower values, and no fluctuations were detected. The rapid and sustained accumulation of GALA-LPs in the lung, with minimal aggregate formation, indicates that the lung endothelium is targeted *via* a specific mechanism.

Cellular Uptake Mechanism. To determine cell specificity for the association of GALA-LPs, the cellular uptake of the GALA-LPs was evaluated using normal human lung microvascular endothelial cells (HMVEC-L), as well as other types of human cell lines. LPs and GALA-LPs were fluorescently labeled by incorporating *N*-(7-nitro-2,1,3-benzoxadiazol-4-yl)dioleoylphosphatidylethanolamine (NBD-DOPE). The cellular uptake of NBD-labeled LPs and GALA-LPs was analyzed by fluorescence-activated cell sorting (FACS), and the relative uptake of GALA-LPs to that of LPs ($F_{GALA\text{-}LPs/LPs}$) was then calculated as an index for the selectivity of GALA-mediated uptake induction (Figure 2A). The $F_{GALA\text{-}LPs/LPs}$ value was significantly higher in endothelium-derived cells, such as HMVEC-L and HUVEC, than in nonendothelial cells (*i.e.*, HepG2, A549, and HeLa cells). Moreover, a competition existed between the GALA-mediated uptake of liposomes by HMVEC-L and preincubated Chol-GALA. The competition was dose-dependent, with IC_{50} values of approximately 1 μM (Figure 2B). These collective data support the conclusion that GALA-LPs recognize a specific molecule on the surface of endothelial cells (*i.e.*, HMVEC-L).

Previous studies revealed that HA2 plays a key role in this process and that it has an affinity for cell surface sugar chains that are terminated with sialic acid.[22−24] Since the GALA was originally designed to mimic the function of HA, we assumed that it might recognize the sialic acid-terminated sugar chain as efficiently as HA2. To address this issue, the cellular uptake of the rhodamine-labeled liposomes by HMVEC-L was evaluated by confocal laser scanning microscopy in the presence or absence of a variety of lectins. The cellular uptake of GALA-LPs was blocked in the presence of the 1 or 10 μM levels of lectins, such as *Maackia amurensis* agglutinin (MAM)[25,26] or *Sambucus sieboldiana* Agglutinin (SSA),[27] which have a high affinity for sialic acid-α2,3-galactose (SAα2,3Gal) or SAα2,6Gal, respectively (Figure 2C, Figure S2). The inhibitory effect of these lectins was minimal in the case of cation-LPs (Figure S3), indicating that the inhibition of the uptake of GALA-LPs by MAM and SSA does not appear to be due to a nonspecific perturbation of cellular function. Moreover,

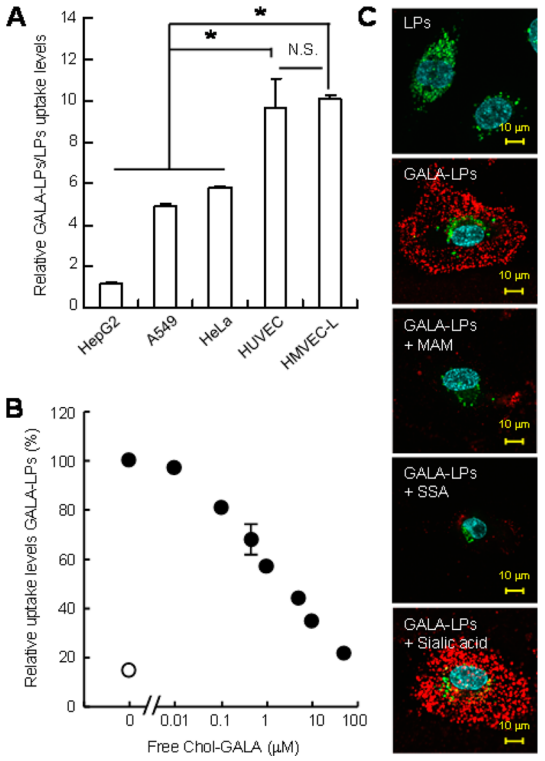

Figure 2. Influenza virus-like active targeting of endothelial cells of GALA-modified LPs. (A) Relative cellular uptake of GALA-LPs to that for LPs by nonendothelial cells (HepG2, A549, and HeLa) and endothelial cells (HMVEC-L and HUVEC). The cellular uptake of NBD-labeled LPs and GALA-LPs was analyzed by FACS, and the relative uptake of GALA-LPs compared to that of LPs ($F_{GALA\text{-}LPs/LPs}$) was then calculated. The relative mean fluorescent intensity is shown as the mean ± SE (n = 3−4). Statistical differences were evaluated by one-way ANOVA followed by Dunnett's test (*p < 0.01 *vs* nonendothelial cells). (B) Inhibition of the intracellular uptake of GALA-LPs by Chol-GALA. The cellular uptake of GALA-LPs by HMVEC-L was determined by FACS at 1 h after incubation with GALA-LPs in the presence of Chol-GALA (0.01−50 μM). The vertical axis shows the relative uptake normalized by those GALA-LPs in the absence of Chol-GALA. Open circles show the uptake of LPs without treatment with Chol-GALA. The values are shown as the mean ± SE (n = 3−5). (C) Inhibition of the cellular uptake of GALA-LPs. The HMVEC-L was preincubated with 10 μM lectins, *Maackia amurensis* agglutinin (MAM) and *Sambucus sieboldiana* agglutinin (SSA), and *N*-acetylneuraminic acid, and the cells were subsequently incubated with rhodamine-labeled GALA-LPs for 2 h. Lysosomes and cell nuclei were stained with LysoTracker Green and Hoechst 33342. Rhodamine signals, LysoTracker Green, and Hoechst 33342 signals are colored red, green, and blue, respectively.

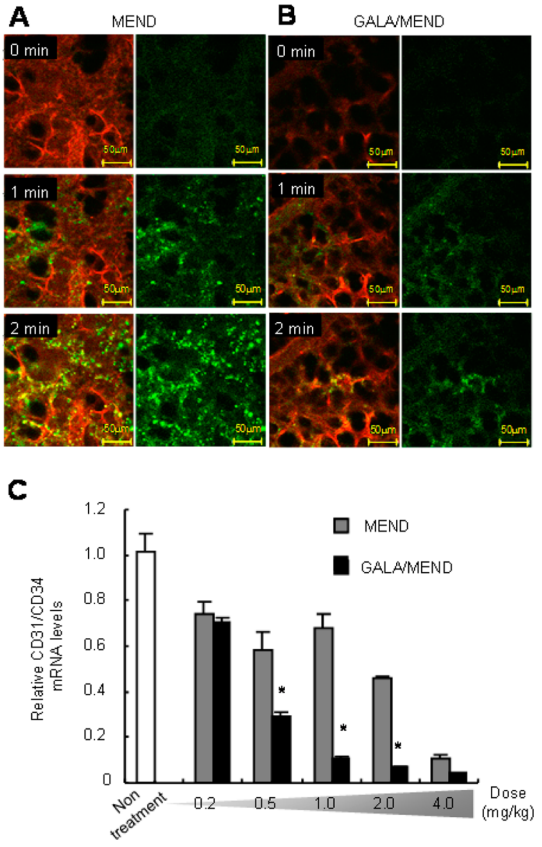

Figure 3. *In vivo* lung accumulation and gene knockdown of the GALA/MEND. Intravital confocal microvideography visualizing the accumulation of MEND (A) and GALA/MEND (B) in mouse pulmonary microvessels. Vasculature was stained with Evans Blue dye. MEND encapsulating Cy3-labeled siRNA was intravenously administered (1.0 mg siRNA/kg) at 60 s (second cycle) after initiating video acquisition. Image sequences were acquired in the video-idle cycle (10 s of acquisition at 30 frames/s, followed by 50 s without acquisition) for a 5 min period. The sequences of images were extracted from Supplemental Movies 4 and 5. (C) Dose-dependent gene knockout activity of MEND and GALA/MEND. MEND (gray bars) and GALA/MEND (solid bars) encapsulating anti-CD31 siRNA were iv administered at 0.2−4.0 mg siRNA/kg. CD31 mRNA levels in lungs were determined by TaqMan real-time PCR. As an internal control, the mRNA expression of CD34 was also determined. Relative expression of CD31/CD34 mRNA levels are shown as the mean ± SE (n = 3−7). The data of administered 4.0 mg siRNA/kg in GALA/MEND are n = 2. Statistical differences in each dose were evaluated by one-way ANOVA followed by Dunnett's test (*p < 0.01 *vs* MEND).

inhibition by *N*-acetylneuraminic acid, a common type of sialic acid, was poor.[28] These data collectively indicate that GALA-LPs, like the influenza virus, recognize a pattern of sugar chains, but not terminal sialic acid residues.

IVCLSM Imaging for the Dynamic Flow of MENDs in Pulmonary Blood Vessels. This system was tested for delivering siRNA to the lung endothelium. We prepared a MEND whose fundamental elements were a negatively charged complex of siRNA and polyethyleneimine (PEI), encapsulated in a cationic liposomal envelope. In the siRNA delivery, we have used cationic lipid composed of DOTMA, EPC, and Chol, since the electrostatic interaction between the cationic lipid bilayer and the negatively charged siRNA/PEI core particle is a crucial driving force for effective packaging. While the overall MEND was highly positively charged (+29 ± 2 mV), GALA modification significantly decreased its ζ-potential to +15 ± 2 mV.

The dynamic accumulation of Cy3-labeled siRNA encapsulated in the MEND and the GALA-modified MEND (GALA/MEND) by the lung was visualized in

TABLE 1. Biochemical Examination of Blood from Mice after the Administration of MEND at 2.0 mg siRNA/kg[a]

sample	AST (UI/L)	ALT (UI/L)	LDH (UI/L)	ALP (UI/L)	ChE (UI/L)	γ-GTP (UI/L)	CK (UI/L)	LIP (UI/L)	GLU (mg/dL)
no treatment	39 (3)	21 (2)	242 (15)	547 (13)	2014 (127)	0.0 (0.0)	89 (10)	42 (1)	282 (7)
MEND	78 (22)	42 (13)	447 (103)	444 (30)	2509 (216)	0.0 (0.0)	119 (24)	38 (3)	264 (4)
GALA-MEND	65 (7)	34 (16)	303 (55)	507 (10)	2289 (66)	0.0 (0.0)	106 (14)	33 (5)	356 (110)

sample	T-Cho (mg/dL)	T-Cho (mg/dL)	PL (mg/dL)	NEFA (mEq/L)	TP (g/dL)	ALB (g/dL)	GLB (g/dL)	A/G ratio
no treatment	82 (5)	69 (4)	172 (9)	0.48 (0.05)	4.6 (0.1)	1.5 (0.0)	1.0 (0.0)	0.49 (0.00)
MEND	105 (2)	75 (18)	194 (12)	0.53 (0.05)	4.8 (0.1)	1.5 (0.0)	1.1 (0.0)	0.47 (0.01)
GALA-MEND	96 (13)	44 (11)	182 (27)	0.49 (0.08)	4.7 (0.2)	1.5 (0.0)	1.1 (0.0)	0.49 (0.01)

sample	UN (mg/dL)	CRE (mg/dL)	T-Bil (mg/dL)	Ca (mg/dL)	IP (mg/dL)	Na (mEq/L)	K (mEq/L)	Cl (mEq/L)
no treatment	26 (2)	0.07 (0.01)	0.09 (0.01)	9.2 (0.1)	8.0 (0.5)	150 (1)	4.0 (0.1)	113 (0)
MEND	25 (3)	0.07 (0.01)	0.10 (0.02)	9.2 (0.2)	8.3 (0.2)	150 (1)	4.4 (0.17)	115 (1)
GALA-MEND	21 (0)	0.06 (0.01)	0.11 (0.02)	9.1 (0.1)	8.2 (0.3)	151 (1)	4.45 (0.11)	115 (1)

[a] Mice were intravenously injected with MEND and GALA/MEND encapsulating anti-CD31 siRNA (2.0 mg siRNA/kg). After 24 h, blood samples were collected for biochemical examination. AST, aspartate aminotransferase; ALT, alanine aminotransferase; LDH, lactate dehydrogenase; ALP, alkaline phosphatase; ChE, cholinesterase; γ-GTP, γ-glutamyltranspeptidase; CK, creatine kinase; LIP, lipase; GLU, glucose; T-Cho, total cholesterol; TG, triglyceride; PL, phospholipid; NEFA, nonesterified fatty acid; TP, total protein; ALB, albumin; UN, urea nitrogen; CRE, creatinine; T-Bil, total bilirubin; Ca, calcium; IP, inorganic phosphorus; Na, sodium; K, potassium; Cl, chloride.

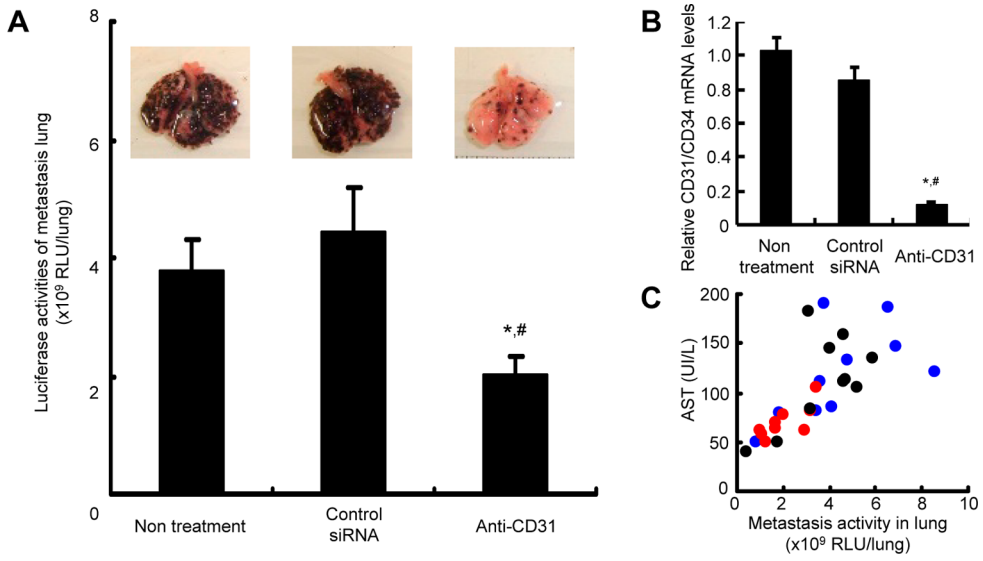

Figure 4. Suppression of the progression of pulmonary metastasis by the administration of GALA/MEND. C57BL/6 mice were challenged with 2 $\times$ 10^5 B16F10-luc2 at day 0 to establish experimental pulmonary metastasis. GALA/MEND encapsulating negative controlled siRNA (anti-GL3) or anti-CD31 siRNA (1.0 mg siRNA/kg) was administered at 3-day intervals from day 1 to day 16. The mice were sacrificed at day 17, and pulmonary metastasis (A), silence activity (B), and serum AST levels (C) were evaluated. (A) Pulmonary metastasis was evaluated using GL4 activity as an index of tumor growth. The values are represented as the mean RLU per lung $\pm$ SE (n = 9−10). (B) The relative mRNA expression of CD31 to that of CD34 as the mean $\pm$ SE (n = 9−10). (C) Interindividual correlation between the progression of lung metastasis and serum AST. The serum AST levels in each mouse were plotted against the progression of intrapulmonary metastasis in terms of the GL4 activity. Symbols are no treatment (black), control siRNA (blue), and anti-CD31 siRNA (red). Statistical differences were evaluated by one-way ANOVA followed by Dunnett's test (*p < 0.05 *vs* nontreatment, $^{\#}p$ < 0.05 *vs* control siRNA).

living animals. The alveolar capillaries were visualized after the intravenous administration of Evans Blue dye, and the MEND or GALA/MEND encapsulating Cy3-labeled siRNA was then administered to the mice (1.0 mg siRNA/kg) *via* a tail vein catheter. Alveolar capillaries of mice lungs were directly observed using IVRTCLSM without any tissue sampling or fixation procedures. In the case of the MEND, siRNA flowed into the lung in the form of large aggregates on the micrometer scale, which then accumulated in the blood vessels (Supplemental Movie 4 and Figure 3A). In contrast, the GALA/MEND flowed in a lung capillary without forming aggregates and gradually accumulated along a blood vessel (Supplemental Movie 5 and Figure 3B). The decrease in particle aggregation as the result of GALA modification was also quantitatively confirmed by calculating the CV of the Cy3 fluorescence signal (Figure S4). After 1 h, siRNA signals in lung capillaries appeared as dispersed signals (Figure S5). The flow of GALA/MEND without aggregation in an

earlobe blood vessel was also confirmed by IVRTCLSM (Figure S6). These data revealed the additional merit in the use of GALA: modification of the peptide may shield the cationic particle from associating with blood serum components, most likely because of the formation of a negatively charged layer on the surface of the particle.

Gene Knockdown in Pulmonary Endothelium. Subsequently, the gene knockdown effect was evaluated using CD31 as an endothelial cell-specific marker gene. siRNA against CD31 was encapsulated into the MENDs or GALA-MEND and intravenously administered to mice at a dose of 0.5−4.0 mg siRNA/kg. At 24 h after the injection, the relative mRNA expression levels of CD31 to CD34 were determined by quantitative RT-PCR. While a significant gene knockdown was observed at a dose of >2.0 mg siRNA/kg in the MEND, significant RNA interference was efficiently achieved at a dose of 0.5 mg siRNA/kg in the GALA/MEND (Figure 3C). Lung-specific gene knockdown was also observed (Figure S7). Furthermore, the system is more efficient compared with AtuPLEX, a technology that is currently being evaluated in phase I clinical trials. In the latter case, an approximately 60% gene knockdown was achieved after a bolus administration of 2.8 mg siRNA/kg on four consecutive days.[29] From the toxicological point of view, the administration of the GALA/MEND (2.0 mg siRNA/kg) had no effect on the serum levels of biomarkers at 1 day postadministration (Table 1).

Antitumor Effect. Recent studies demonstrated that the knockout of the CD31 gene or the administration of an anti-CD31 antibody prevented the metastatic progression of advanced melanoma, likely due to the perturbation of the tumor microenvironment.[30] Luciferase (GL4) stably expressed by a melanoma, B16-F10 (B16-F10-luc2), was iv administered to mice (day 0), and on the next day, GALA/MEND encapsulating anti-CD31 siRNA was repeatedly injected (1.0 mg siRNA/kg) six times at 3-day intervals. At day 17, metastasis was significantly inhibited by approximately 50% compared with the control groups (Figure 4A). Under this circumstance, a more than 80% gene knockdown was achieved against the nontreated and anti-GL3 siRNA-treated groups (Figure 4B). During this experiment, no decrease in body weight or increase in serum ALT was observed (Figure S8). Thus, the repeated injection of the GALA/MEND was intrinsically tolerated by the mice. Meanwhile, the serum level of AST, a marker for hepatic metastasis, was suppressed by the administration of anti-CD31 siRNA (Figure S8B). Moreover, serum AST levels were well correlated with the progression of metastasis (Figure 4C). Thus, as a secondary effect, the suppression of lung metastasis in the anti-CD31 siRNA-treated group might result in the prevention of hepatic metastasis in the end stage.

CONCLUSION

The findings of this study indicate that the GALA/MEND is a highly potent artificial carrier of nucleic acids for targeting the lung endothelium, whose key element, GALA, plays a key role in the recognition of a sialic acid-terminated sugar chain for cellular uptake and membrane fusion for the endosomal release of the encapsulated siRNA. This artificial influenza virus-like vector targeting the lung endothelium opens a new-generation therapeutic approach for satisfying unmet medical needs in curing lung diseases.

METHODS

General Procedures. Cholesterol, rhodamine-dioleoylphosphatidylethanolamine (Rho-DOPE), and NBD-DOPE were purchased from AVANTI Polar Lipids (Alabaster, AL, USA). Egg phosphatidylcholine was purchased from NOF Co., Ltd. (Tokyo, Japan). DOTMA was purchased from Tokyo Chemical Industry Co., Ltd. (Tokyo, Japan). Stearyl-polyethylene glycol 2000 and polyethyleneimine (branch type, M_w. av 10 000) were purchased from Wako Pure Chemicals (Tokyo, Japan). [Cholesteryl-1,2-^{3}H(N)]-cholesteryl hexadecyl ether ([^{3}H]CHE) was purchased from PerkinElmer Life Science Japan (Tokyo, Japan). *Maackia amurensis* agglutinin and *Sambucus sieboldiana* agglutinin were purchased from J-OIL MILLS, Inc. (Tokyo, Japan). Cholesterol-GALA was synthesized as described previously.[31]

All animal experimental procedures were carried out in accordance with the Guide for the Care and Use of Laboratory Animals as stated by the National Institutes of Health.

Preparation of Liposomes. Lipids composed of 275 nmol (for *in vitro*) or 1320 nmol (for *in vivo*) of EPC/Chol/STR-mPEG (7/3/0.5) and DOTMA/EPC/Chol/STR-mPEG (3/4/3/0.5) were dissolved in chloroform/ethanol (1:1) to prepare the LPs and cation-LPs. For the preparation of GALA-LPs, 2 mol % Chol-GALA was added to the lipid composition. These lipid solutions were evaporated, resulting in the formation of a lipid film. Thereafter, 10 mM HEPES solution (pH = 7.4) containing 5% glucose was added, and the preparation incubated for 15 min to hydrate the lipid film. The glass tube was sonicated for approximately 1 min in a bath-type sonicator (Aiwa, Japan). To label the LPs with rhodamine or NBD, rhodamine-DOPE or NBD-DOPE was also incorporated into the lipid composition. The average diameter and the zeta-potentials of the liposomes were determined using a Zetasizer Nano ZS ZEN3600 (Malvern Instruments, Worchestershire, UK).

Preparation of MENDs. The sequences of the siRNA used in the present study are summarized in Table S2. In preparing the CD31-targeted siRNA, three equal sets of siRNAs were mixed. siRNA and PEI were first dissolved in a 10 mM HEPES buffer (pH 7.4) that contained 5% glucose. Then 200 μL of PEI (0.125 mg/mL) was added to the 300 μL of siRNA (0.33 mg/mL) to form a complex at a nitrogen/phosphate ratio of 1.8. A lipid film was formed by the evaporation of a chloroform/ethanol solution containing 1.32 μmol of total lipids of DOTMA/Chol/EPC/STR-mPEG (30:40:30:5). To prepare the GALA/MEND, 2 mol % Chol-GALA was added to the lipid composition. The siRNA/PEI complex was applied to the lipid film, followed by incubation for 15 min at room temperature to hydrate the lipids. To encapsulate the siRNA/PEI complex in the lipid, the lipid film was sonicated for approximately 1 min in a bath-type sonicator.

Evaluation of the Organ Concentration of Liposomes. The lipid bilayers of MENDs were labeled with a trace amount of [^{3}H]CHE (0.5 μCi per 412.5 nmol of total lipid) by incorporating [^{3}H]CHE into the lipid film. The liposomes were injected into 5-week-old ICR (Japan SLC, Shizuoka, Japan) mice *via* the tail vein with 26.4 μmol lipid/kg. At the indicated times, the mice were

sacrificed, and lung, liver, and spleen samples were collected. After weighing the samples, the organ samples were solubilized in Soluene 350 overnight at 50 °C and were then decolorized by treatment with H_2O_2. Radioactivities were determined by liquid scintillation counting (LSC-6100 (ALOKA)), with Hionic-Fluor. The organ concentration is represented as the percent of injected dose per gram of organ tissue (%ID/g organ).

Flow Cytometry for the Cellular Uptake of LPs. NBD-labeled LPs were prepared by incorporating 2 mol % of NBD-DOPE into the lipid composition. NBD-labeled liposomes (55 nmol of total lipids) were incubated with 2×10^5 cells (HMVEC-L, HUVEC, HeLa, A549, and HepG2) seeded on a six-well culture dish in serum-free Krebs-Henseleit buffer for 1 h at 37 °C. For the inhibition studies using Chol-GALA as an inhibitor, HMVEC-L cells were preincubated with Chol-GALA (0.01−50 μM) for 15 min, and NBD-labeled liposomes were then applied to the cell culture, as described above. For flow cytometry analyses, cells were washed once with PBS supplemented with heparin (20 units/mL) and then trypsinized and collected in an Eppendorf tube. The contents of the tube were then washed two additional times by reprecipitation of the cells by centrifugation (1500 rpm, 4 °C, 5 min), followed by resuspension in 1 mL of heparin-PBS. Finally, the cells were suspended in 1 mL of PBS. Cells were analyzed by flow cytometry (FACScan, Becton Dickinson).

Intracellular Observation of LPs Using Confocal Laser Scanning Microscopy. Rhodamine-labeled LPs were prepared by incorporating 1 mol % of rhodamine-DOPE into the lipid composition. Rhodamine-labeled liposomes (27.5 nmol of total lipids) were incubated with 4×10^4 HMVEC-L cells seeded on 35 mm dishes (IWAKI, Osaka, Japan) in serum-free Krebs-Henseleit buffer for 2 h at 37 °C. To evaluate the inhibitory effect of lectins, HMVEC-L cells were preincubated with 1 or 10 μM lectins (MAM and SSA) for 30 min. Thereafter, unbound MAM and SSA were washed three times with Krebs-Henseleit buffer before incubation with rhodamine-labeled liposomes. Finally, sialic acid inhibition was demonstrated by preincubation with 1 or 10 μM *N*-acetylneuraminic acid for 30 min, followed by incubation with rhodamine-labeled LPs. The cells were observed by confocal laser scanning microscopy (CLSM) after staining the lysosomes and cell nuclei.

Thirty minutes and 10 minutes before acquiring the fluorescence images, lysosomes and cell nuclei were stained with Lysotracker Green (Invitrogen Co, Carland, CA, USA) and Hoechst 33342 (Sigma-Aldrich Co., St. Louis, MO, USA). After the incubation, the cells were washed with Krebs-Henseleit buffer and then observed by CLSM (FV10i-LIV; Olympus Corporation, Tokyo, Japan). The cells were excited with a 352 nm light, a 473 nm light, and 559 nm light from an LD laser. Images were obtained using an FV10i-LIV equipped with a water-immersion objective lens (UPlanSApo 60×/NA 1.2) and a dichroic mirror (DM405/473/559/635). The three fluorescence detection channels (Ch) were set to the following filters: Ch1: 455 (blue) for Hoechst 33342, Ch2: 490−540 (green) for Lysotracker Green, Ch3: 570−620 (red) for rhodamine.

IVRTCLSM Analysis. Eight-week-old female BALB/c nude mice (Oriental Yeast Co., Ltd., Tokyo, Japan) were anesthetized with 2.0−3.0% isoflurane (Abbott Japan Co., Ltd., Tokyo, Japan) using a Univenter 400 anesthesia unit (Univentor Ltd., Zejtun, Malta). The mice were then subjected to lateral tail vein catheterization with a 30-gauge needle (Dentronics Co., Ltd., Tokyo, Japan) connected to a nontoxic, medical-grade polyethylene tube (Natsume Seisakusho Co., Ltd., Tokyo, Japan).

Methods for the IVRTCLSM analysis in earlobe blood flow have been described previously. In this analysis, LPs labeled by the incorporation of 0.1 mol % of Rho-DOPE were iv administered at a dose of 528 nmol total lipid. For the intrapulmonary IVRTCLSM of MEND, a small transthoracic window was made using a Surgitron radio frequency surgical device (Ellman International Inc., Oceanside, NY, USA) after performing a tracheostomy to secure ventilation. The mice were placed on a temperature-controlled pad (Thermoplate; Tokai Hit Co., Ltd., Shizuoka, Japan) integrated into a customized microscope stage and maintained in a sedated state throughout the period of the measurements. A custom-designed height-adjustable coverslip holder was placed on the lung and then glued in place to provide a flat surface for the objective lens.

Evans Blue dye (8 mg/kg in PBS, Wako Pure Chemical Industries, Ltd., Osaka, Japan), which binds to plasma albumin, was used to stain the vasculature. These dyes were administered in advance to determine the most appropriate site for imaging lung alveolar capillaries. Cy3-labeled siRNA (Hokkaido System Science Co., Ltd., Sapporo, Japan) encapsulated in MEND and GALA/MEND were administered to the mice (1.0 mg siRNA/kg) *via* the tail vein catheter at 60 s (second cycle) after video acquisition was initiated.

The degree of aggregation was quantified by calculating the coefficient of variation (CV) of rhodamine fluorescence, which denotes the ratio of the standard deviation to the mean in the ROI cropped within a vessel region. The calculated CV values were plotted against time.

All picture/movie acquisitions were performed using a Nikon A1R confocal laser scanning microscope system attached to an upright Eclipse FN1 equipped with a CFI Apo 40× WI λS objective (Nikon Corp., Tokyo, Japan). The pinhole diameter was set to result in a 10 μm optical slice. Data were acquired in the video-idle cycle (10 s acquisition at 30 frames/s, followed by 50 s without acquisition) for 10 min.

Analysis of mRNA Expression of CD31. The prepared MEND particles were injected one time into 6-week-old male C57BL/6 mice *via* the tail vein at a dose of 0.5−4.0 mg siRNA/kg. At 24 h after the injection, the mice were sacrificed, and relevant organs collected. The collected lungs were washed with saline and immersed in RNAlater (Ambion) at 4 °C overnight and then stored at −20 °C. Each organ sample was homogenized using a PreCellys (Bertin Technologies, France), and the homogenate was then subjected to total RNA extraction by means of RNeasy (Qiagen). Total RNA (1 μg) was reverse transcribed using a High Capacity RNA-to-cDNA kit (ABI) according to the manufacturer's protocol. A quantitative PCR analysis was performed on 2 ng of cDNA using the TaqMan Gene Expression Master Mix (ABI) and Prism7500 (ABI). The sequences of the set of TaqMan probes are listed in Table S3. The PCR parameters consisted of a primary denaturing at 95 °C × 10 min, followed by 40 cycles of PCR at 95 °C × 15 s, 60 °C × 1 min. The relative amount of target gene was normalized to CD34 mRNA.

Antitumor Effect of GALA/MEND in Lung Metastatic Tumor Models. B16-F10 murine melanoma cells stably expressing luciferase (GL4) (B16-F10-luc2; Caliper Life Sciences, MA, USA) were grown in 10% FBS in RPMI-1640 medium (Invitrogen) for 48 h. On day 0, 2×10^5 B16-F10-luc2 cells in 100 μL of PBS were iv injected. From day 1, 200 μL of control siRNA (anti-GL3) or anti-CD31 siRNA encapsulated in GALA/MEND was injected at a dose of 1 mg siRNA/kg at 3-day intervals. On day 17, the mice were sacrificed, and the lungs collected. The lung tissue was divided into two fractions, and tumor metastasis and mRNA expression of CD31 were analyzed. For the quantification of tumor metastasis, a portion of the collected lungs was completely homogenized using a Polytron homogenizer (Kinematica, Littan, Switzerland) in 1 mL of lysis buffer (100 mM Tris−HCl, 2 mM EDTA, 0.1% Triton X-100, pH 7.8). After centrifugation at 13 000 rpm for 10 min at 4 °C, the luciferase activity in a 20 μL aliquot of the cell lysate was then measured using a luminometer (Luminescencer-PSN, ATTO, Japan). Luciferase activities are expressed as relative light units (RLU) per whole lung.

To evaluate liver toxicity, blood samples were collected at day 17 and allowed to stand at 4 °C until coagulation was complete. Serum was obtained by centrifuging the coagulated blood at 10 000 rpm at 4 °C for 10 min. Serum alanine transaminase (ALT) and aspartate amino transferase (AST) activities were determined using a commercially available kit (Wako Chemicals, Osaka, Japan).

Conflict of Interest: The authors declare no competing financial interest.

Acknowledgment. This work was supported, in part, by Core Research Program for Evolutional Science and Technology (CREST) from the Japan Science and Technology Corporation (JST), and in part by Funding Program for Next Generation World-Leading Researchers (NEXT Program). The authors thank Miss Y. Naraki and Mrs. K. Nakamura (Space-Time Inc.) for their support in preparing the graphical illustrations. Finally, the authors thank Dr. M. S. Feather for his helpful advice in writing the English manuscript.

Supporting Information Available: Figures S1–S8, Tables S1–S3, and Movies S1–S5. These materials are available free of charge *via* the Internet at http://pubs.acs.org.

REFERENCES AND NOTES

1. Png, K. J.; Halberg, N.; Yoshida, M.; Tavazoie, S. F. A Microrna Regulon That Mediates Endothelial Recruitment and Metastasis by Cancer Cells. *Nature* **2012**, *481*, 190–194.
2. Matsuda, N.; Takano, Y.; Kageyama, S.; Hatakeyama, N.; Shakunaga, K.; Kitajima, I.; Yamazaki, M.; Hattori, Y. Silencing of Caspase-8 and Caspase-3 by RNA Interference Prevents Vascular Endothelial Cell Injury in Mice with Endotoxic Shock. *Cardiovasc. Res.* **2007**, *76*, 132–140.
3. McDonald, R. A.; Hata, A.; MacLean, M. R.; Morrell, N. W.; Baker, A. H. MicroRNA and Vascular Remodelling in Acute Vascular Injury and Pulmonary Vascular Remodelling. *Cardiovasc. Res.* **2012**, *93*, 594–604.
4. Gaine, S. P.; Rubin, L. J. Primary Pulmonary Hypertension. *Lancet* **1998**, *352*, 719–725.
5. Aleku, M.; Fisch, G.; Mopert, K.; Keil, O.; Arnold, W.; Kaufmann, J.; Santel, A. Intracellular Localization of Lipoplexed Sirna in Vascular Endothelial Cells of Different Mouse Tissues. *Microvasc. Res.* **2008**, *76*, 31–41.
6. Liu, F.; Qi, H.; Huang, L.; Liu, D. Factors Controlling the Efficiency of Cationic Lipid-Mediated Transfection *in Vivo via* Intravenous Administration. *Gene Ther.* **1997**, *4*, 517–523.
7. Regnstrom, K.; Ragnarsson, E. G.; Fryknas, M.; Koping-Hoggard, M.; Artursson, P. Gene Expression Profiles in Mouse Lung Tissue after Administration of Two Cationic Polymers Used for Nonviral Gene Delivery. *Pharm. Res.* **2006**, *23*, 475–482.
8. Park, M. R.; Kim, H. W.; Hwang, C. S.; Han, K. O.; Choi, Y. J.; Song, S. C.; Cho, M. H.; Cho, C. S. Highly Efficient Gene Transfer with Degradable Poly(Ester Amine) Based on Poly(Ethylene Glycol) Diacrylate and Polyethylenimine *in Vitro* and *in Vivo*. *J. Gene Med.* **2008**, *10*, 198–207.
9. Mahato, R. I.; Anwer, K.; Tagliaferri, F.; Meaney, C.; Leonard, P.; Wadhwa, M. S.; Logan, M.; French, M.; Rolland, A. Biodistribution and Gene Expression of Lipid/Plasmid Complexes after Systemic Administration. *Hum. Gene Ther.* **1998**, *9*, 2083–2099.
10. Li, S.; Tseng, W. C.; Stolz, D. B.; Wu, S. P.; Watkins, S. C.; Huang, L. Dynamic Changes in the Characteristics of Cationic Lipidic Vectors after Exposure to Mouse Serum: Implications for Intravenous Lipofection. *Gene Ther.* **1999**, *6*, 585–594.
11. Wright, M. J.; Rosenthal, E.; Stewart, L.; Wightman, L. M.; Miller, A. D.; Latchman, D. S.; Marber, M. S. Beta-Galactosidase Staining Following Intracoronary Infusion of Cationic Liposomes in the *in Vivo* Rabbit Heart Is Produced by Microinfarction Rather Than Effective Gene Transfer: A Cautionary Tale. *Gene Ther.* **1998**, *5*, 301–308.
12. Chen, J.; Wharton, S. A.; Weissenhorn, W.; Calder, L. J.; Hughson, F. M.; Skehel, J. J.; Wiley, D. C. A Soluble Domain of the Membrane-Anchoring Chain of Influenza Virus Hemagglutinin (HA2) Folds in Escherichia coli into the Low-pH-Induced Conformation. *Proc. Natl. Acad. Sci. U.S.A.* **1995**, *92*, 12205–12209.
13. Jardetzky, T. S.; Lamb, R. A. Virology: A Class Act. *Nature* **2004**, *427*, 307–308.
14. Sakurai, Y.; Hatakeyama, H.; Sato, Y.; Akita, H.; Takayama, K.; Kobayashi, S.; Futaki, S.; Harashima, H. Endosomal Escape and the Knockdown Efficiency of Liposomal-siRNA by the Fusogenic Peptide Shgala. *Biomaterials* **2011**, *32*, 5733–5742.
15. Kusumoto, K.; Akita, H.; El-Sayed, A.; Harashima, H. Effect of the Anchor in Polyethylene Glycol-Lipids on the Transfection Activity of PEGylated Cationic Liposomes Encapsulating DNA. *Biol. Pharm. Bull.* **2012**, *35*, 445–448.
16. Li, W.; Nicol, F.; Szoka, F. C., Jr. GALA: A Designed Synthetic pH-Responsive Amphipathic Peptide with Applications in Drug and Gene Delivery. *Adv. Drug Delivery Rev.* **2004**, *56*, 967–985.
17. Kakudo, T.; Chaki, S.; Futaki, S.; Nakase, I.; Akaji, K.; Kawakami, T.; Maruyama, K.; Kamiya, H.; Harashima, H. Transferrin-Modified Liposomes Equipped with a pH-Sensitive Fusogenic Peptide: An Artificial Viral-Like Delivery System. *Biochemistry* **2004**, *43*, 5618–5628.
18. Ishitsuka, T.; Akita, H.; Harashima, H. Functional Improvement of an IRQ-PEG-MEND for Delivering Genes to the Lung. *J. Controlled Release* **2011**, *154*, 77–83.
19. Matsumoto, Y.; Nomoto, T.; Cabral, H.; Matsumoto, Y.; Watanabe, S.; Christie, R. J.; Miyata, K.; Oba, M.; Ogura, T.; Yamasaki, Y.; *et al.* Direct and Instantaneous Observation of Intravenously Injected Substances Using Intravital Confocal Micro-Videography. *Biomed. Opt. Express* **2010**, *1*, 1209–1216.
20. Hatanaka, K.; Asai, T.; Koide, H.; Kenjo, E.; Tsuzuku, T.; Harada, N.; Tsukada, H.; Oku, N. Development of Double-Stranded siRNA Labeling Method Using Positron Emitter and Its *in Vivo* Trafficking Analyzed by Positron Emission Tomography. *Bioconjugate Chem.* **2010**, *21*, 756–763.
21. Nomoto, T.; Matsumoto, Y.; Miyata, K.; Oba, M.; Fukushima, S.; Nishiyama, N.; Yamasoba, T.; Kataoka, K. *In Situ* Quantitative Monitoring of Polyplexes and Polyplex Micelles in the Blood Circulation Using Intravital Real-Time Confocal Laser Scanning Microscopy. *J. Controlled Release* **2011**, *151*, 104–109.
22. Daniels, R. S.; Douglas, A. R.; Skehel, J. J.; Wiley, D. C.; Naeve, C. W.; Webster, R. G.; Rogers, G. N.; Paulson, J. C. Antigenic Analyses of Influenza Virus Haemagglutinins with Different Receptor-Binding Specificities. *Virology* **1984**, *138*, 174–177.
23. Yamada, S.; Suzuki, Y.; Suzuki, T.; Le, M. Q.; Nidom, C. A.; Sakai-Tagawa, Y.; Muramoto, Y.; Ito, M.; Kiso, M.; Horimoto, T.; *et al.* Haemagglutinin Mutations Responsible for the Binding of H5N1 Influenza a Viruses to Human-Type Receptors. *Nature* **2006**, *444*, 378–382.
24. Stevens, J.; Blixt, O.; Tumpey, T. M.; Taubenberger, J. K.; Paulson, J. C.; Wilson, I. A. Structure and Receptor Specificity of the Hemagglutinin from an H5N1 Influenza Virus. *Science* **2006**, *312*, 404–410.
25. Knibbs, R. N.; Goldstein, I. J.; Ratcliffe, R. M.; Shibuya, N. Characterization of the Carbohydrate Binding Specificity of the Leukoagglutinating Lectin from Maackia Amurensis. Comparison with Other Sialic Acid-Specific Lectins. *J. Biol. Chem.* **1991**, *266*, 83–88.
26. Wang, W. C.; Cummings, R. D. The Immobilized Leukoagglutinin from the Seeds of Maackia Amurensis Binds with High Affinity to Complex-Type Asn-Linked Oligosaccharides Containing Terminal Sialic Acid-Linked Alpha-2,3 to Penultimate Galactose Residues. *J. Biol. Chem.* **1988**, *263*, 4576–4585.
27. Takesada, H.; Shibuya, N.; Nagashima, N. The Interaction of Elderberry (Sambucus sieboldiana) Bark Lectin and Sialyloligosaccharides as Detected by 1H-NMR. *J. Biochem.* **1992**, *112*, 143–146.
28. Schauer, R. Achievements and Challenges of Sialic Acid Research. *Glycoconjugate J.* **2000**, *17*, 485–499.
29. Santel, A.; Aleku, M.; Keil, O.; Endruschat, J.; Esche, V.; Fisch, G.; Dames, S.; Loffler, K.; Fechtner, M.; Arnold, W.; *et al.* A Novel siRNA-Lipoplex Technology for RNA Interference in the Mouse Vascular Endothelium. *Gene Ther.* **2006**, *13*, 1222–1234.
30. DeLisser, H.; Liu, Y.; Desprez, P. Y.; Thor, A.; Briasouli, P.; Handumrongkul, C.; Wilfong, J.; Yount, G.; Nosrati, M.; Fong, S.; *et al.* Vascular Endothelial Platelet Endothelial Cell Adhesion Molecule 1 (PECAM-1) Regulates Advanced Metastatic Progression. *Proc. Natl. Acad. Sci. U.S.A.* **2010**, *107*, 18616–18621.
31. Futaki, S.; Ishikawa, T.; Niwa, M.; Kitagawa, K.; Yagami, T. Embodying a Stable Alpha-Helical Protein Structure through Efficient Chemical Ligation *via* Thioether Formation. *Bioorg. Med. Chem.* **1997**, *5*, 1883–1891.